Spatial separation of redox centers for boosting cooperative photocatalytic hydrogen evolution with oxidation coupling of benzylamine over Pt@UiO-66-NH_2@$ZnIn_2S_4$

Lianlian Wang, Yujie Zhao, Bin Zhang, Gaigai Wu, Jie Wu, Hongwei Hou**

Green Catalysis Center, College of Chemistry, Zhengzhou University, Zhengzhou 450001, P. R. China.

*Correspondence:

Jie Wu-Green Catalysis Center, College of Chemistry, Zhengzhou University, Zhengzhou 450001, P. R. China; orcid.org/0000-0001-7746-6640; Email: wujie@zzu.edu.cn

Hongwei Hou-Green Catalysis Center, College of Chemistry, Zhengzhou University, Zhengzhou 450001, P. R. China; orcid.org/0000-0003-4762-0920; Email: houhongw@zzu.edu.cn

Chemicals and materials

All chemicals (analytical grade) were purchased from Fluorochem and used directly without further purification from. Rigaku MiniFlex2 diffractometer operating with Cu Ka source was used to record the powder X-Ray diffraction (XRD). The morphologies of as-prepared samples were characterized via scanning electron microscopy (SEM) (Zeiss Sigma 500 instrument). UV-vis diffuse reflectance spectra were measured in the range of 200-800 nm with a JASCO V-750 UV-vis spectrophotometer. Transmission electron microscope (TEM) and high-resolution TEM (HRTEM) were performed using FEI Tecnai G2 F20 electron microscope. The chemical component and electronic state of the products were examined by X-ray photoelectron spectroscopy (XPS) (Thermo Fischer ESCALAB, US). The N_2 adsorption-desorption isotherms were obtained by the Microtrac BEL Corp surface at 77 K. Electron spin resonance (ESR) technology was obtained by EMXmicro-6/1/P/L, Karlsruhe, Germany instrument to measure free radical signals with 5-dimethyl-1 pyrroline N-oxide (DMPO) or 2,2,6,6-tetramethylpiperidine-nitrogen-oxide (TEMPO) as trapping agents. Catalytic H_2 generation products were analyzed and identified by gas chromatography (Panna A91Plus, Panna AB-5).

The photoluminescence (PL) spectra and time-resolved photoluminescence (TRPL) spectra were obtained on an JASCO FP-8300 fluorescence spectrometers. The decay curves were fitted by a triexponential decay function and the average PL life times ($\tau_{average}$) were calculated according to the following equations:

$$A(t) = A_1 e^{(\frac{t}{\tau_1})} + A_2 e^{(\frac{t}{\tau_2})}$$

$$\tau = \frac{A_1\tau_1^2 + A_2\tau_2^2}{A_1\tau_1 + A_2\tau_2}$$

The band gap values of UiO-66-NH_2 and $ZnIn_2S_4$ can be calculated using the following equation.

$$\alpha h\nu = A\left(h\nu - E_g\right)^n$$

where α, h, *ν*, A, n and E g represent the absorption coefficient, planck constant, light frequency, constant value, n = 1/2 or 2 for direct bandgap or indirect bandgap semiconductors, respectively, and band gap energy of the photocatalyst, respectively. As shown in Figure 4b, the E_g values of UiO-66-NH_2 and $ZnIn_2S_4$ are 2.90 and 2.50 eV, respectively. Furthermore, the potential positions of UiO-66-NH_2 and $ZnIn_2S_4$ were determined by the Mott-Schottky curve (Figure 4c-d). The positive slopes of UiO-66-NH_2 and $ZnIn_2S_4$ indicate that they are both typical n-type semiconductors. The flat band potentials of UiO-66-NH_2 and $ZnIn_2S_4$ are about -0.75 and -1.15 V *vs.* Ag/AgCl. Typically, for n-type semiconductors, the conduction band edge potential is about 0.2 V more negative than the flat band potential of the material. According to the following equation: $E_{VB} = E_{CB} + E_g$, it can be calculated that the LUMO and HUMO values of UiO-66-NH_2 are -0.55 and 2.35 V *vs*. NHE. Likely, the conduction band (CB) level of $ZnIn_2S_4$ is -0.95 V *vs*. NHE, the valence band (VB) potential is calculated as 1.55 V vs. NHE.

Photoelectrochemical tests

The photocurrent measurements and electrochemical impedance spectroscopy (EIS) measurements were obtained via the CHI660E electrochemical workstation (Shanghai Chenhua Apparatus, China) in a standard three-electrode system, in which a saturated silver electrode (Ag/AgCl) was used as the reference electrode and a Pt plate was used as the auxiliary electrode, and Na_2SO_4 solution (0.1 mol L^{-1}) was employed as the electrolyte. The preparation process of working electrode was as follows: 10 mg photocatalyst was dispersed in 1 mL of acetone, and then the suspension was ultrasonically for 20 min. Thereafter, the suspension was dropped on the surface of a 1 × 2 cm^2 fluorine-doped tin oxide (FTO) glass, which was subsequently placed in an oven for 40 °C overnight. In the EIS Nyquist plot and transient photocurrent, initial voltage, alternating voltage and frequency were -0.1 V,

5 mV and 10^5-10^{-2} Hz, respectively. A 300 W xenon lamp was used as the light to obtain a photocurrent spectrum.

Detection experiment of active species

ESR signals were detected by a Bruker A300E spectrometer. At room temperature, 10 mg samples were dispersed in 10 mL methanol by ultrasound. Then, 30 μL suspension was added to 30 μL 50 mM DMPO (5,5-dimethyl-1-pyrroline N-oxide) solution. After mixing and shaking well, the samples were put into the machine for testing $\cdot O_2^-$. In addition, testing h^+ is conducted with the similar method except replacing DMPO with TEMPO (2,2,6,6-tetramethylpiperidine-1-oxyl).

Computational method

We have employed the Vienna Ab Initio Package (VASP)[1,2] to perform all the density functional theory (DFT) calculations within the generalized gradient approximation (GGA) using the PBE[3] formulation. We have chosen the projected augmented wave (PAW) potentials[4,5] to describe the ionic cores and take valence electrons into account using a plane wave basis set with a kinetic energy cutoff of 450 eV. Partial occupancies of the Kohn−Sham orbitals were allowed using the Gaussian smearing method and a width of 0.05 eV. The electronic energy was considered self-consistent when the energy change was smaller than 10-5 eV. A geometry optimization was considered convergent when the force change was smaller than 0.05 eV/Å. Grimme's DFT-D3 methodology was used to describe the dispersion interactions. During structural optimizations, a 2 × 2 × 1 k-point grid in the Brillouin zone was used for k-point sampling.

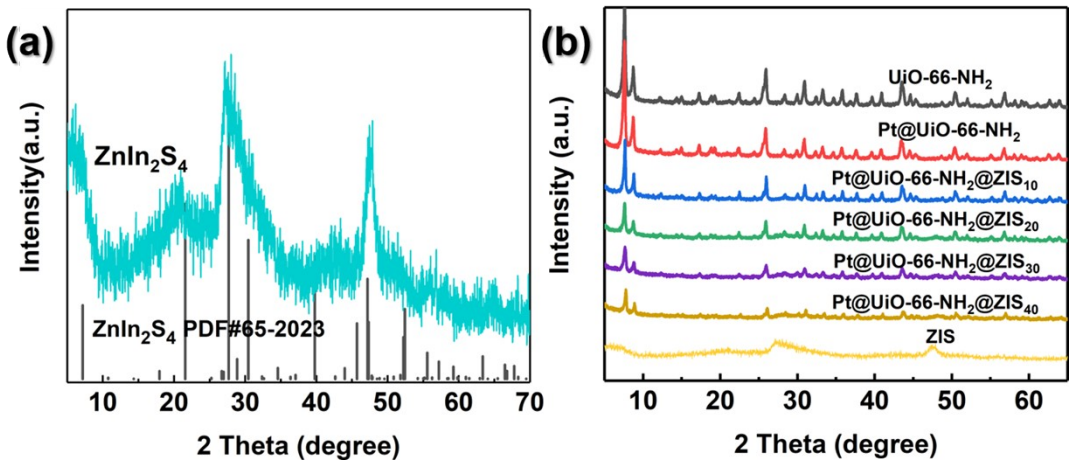

Fig. S1 XRD patterns of $ZnIn_2S_4$ (a) and as-prepared heterostructure composite samples (b).

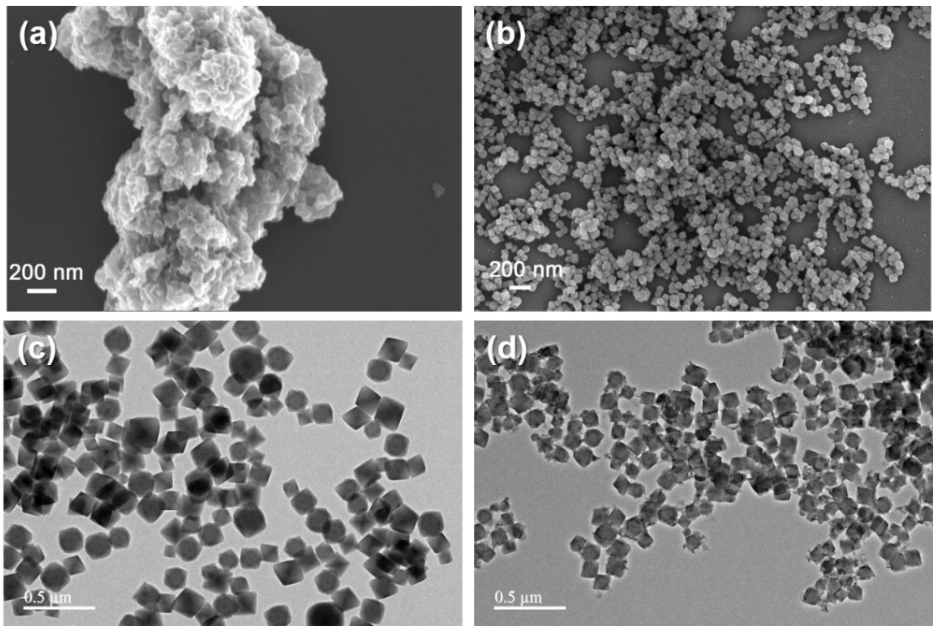

Fig. S2 SEM images of (a) $ZnIn_2S_4$ and (b) UiO-66-NH_2; TEM images of (c) Pt@UiO-66-NH_2 and (d) Pt@UiO-66-NH_2@ZIS.

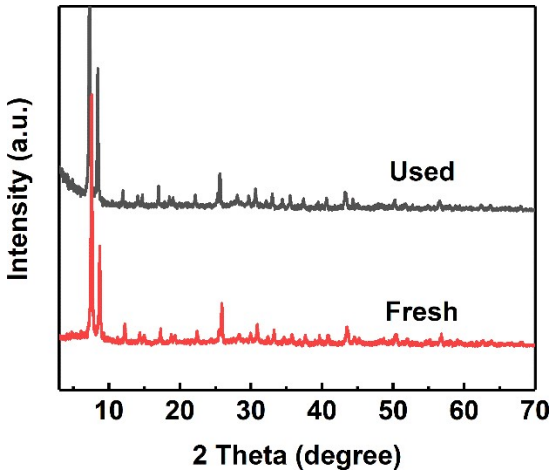

Fig. S3 XRD patterns of the Pt@UiO-66-NH_2@ZIS sample before and after photocatalytic reaction.

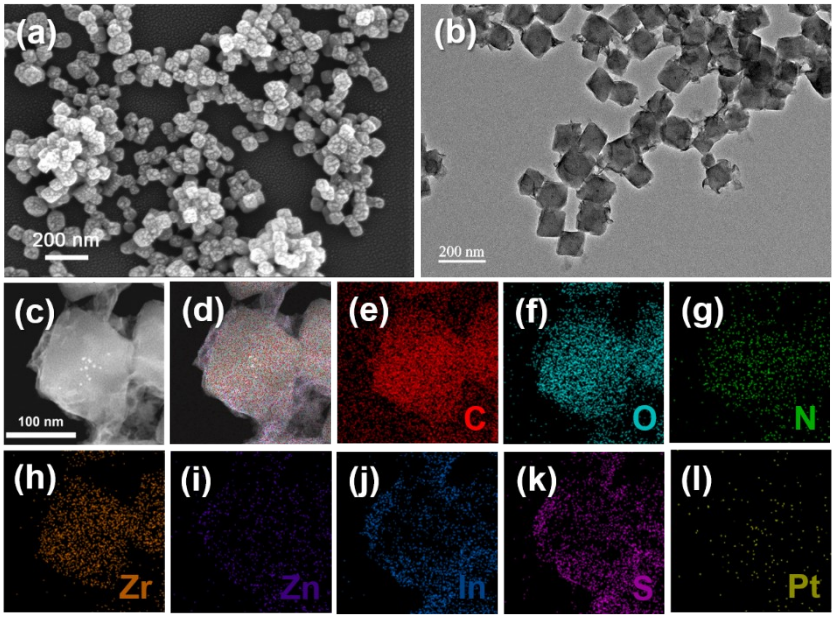

Fig. S4 (a) SEM images, (b) TEM images and (c-l) TEM-EDS images of Pt@UiO-66-NH_2@ZIS sample before and after photocatalytic reaction.

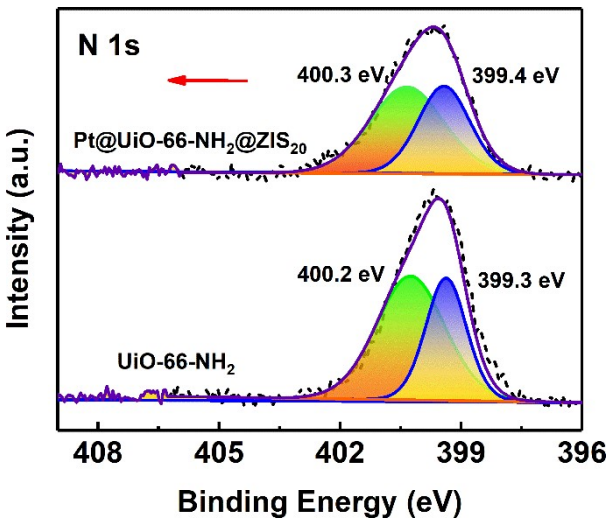

Fig. S5 XPS spectrum of N 1s of Pt@UiO-66-NH_2@ZIS_{20} and UiO-66-NH_2 sample.

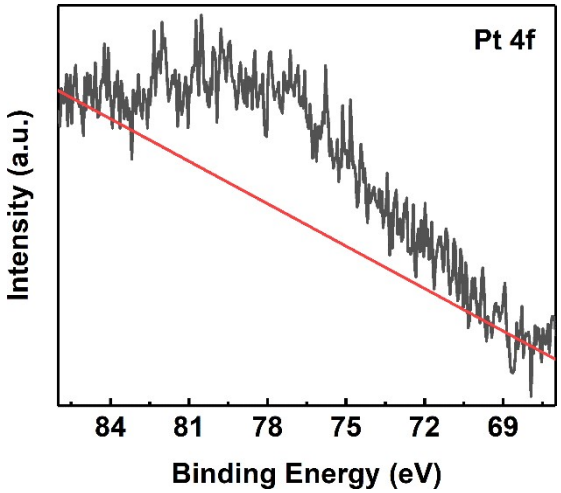

Fig. S6 XPS spectrum of Pt 1s of Pt@UiO-66-NH_2@ZIS_{20} sample.

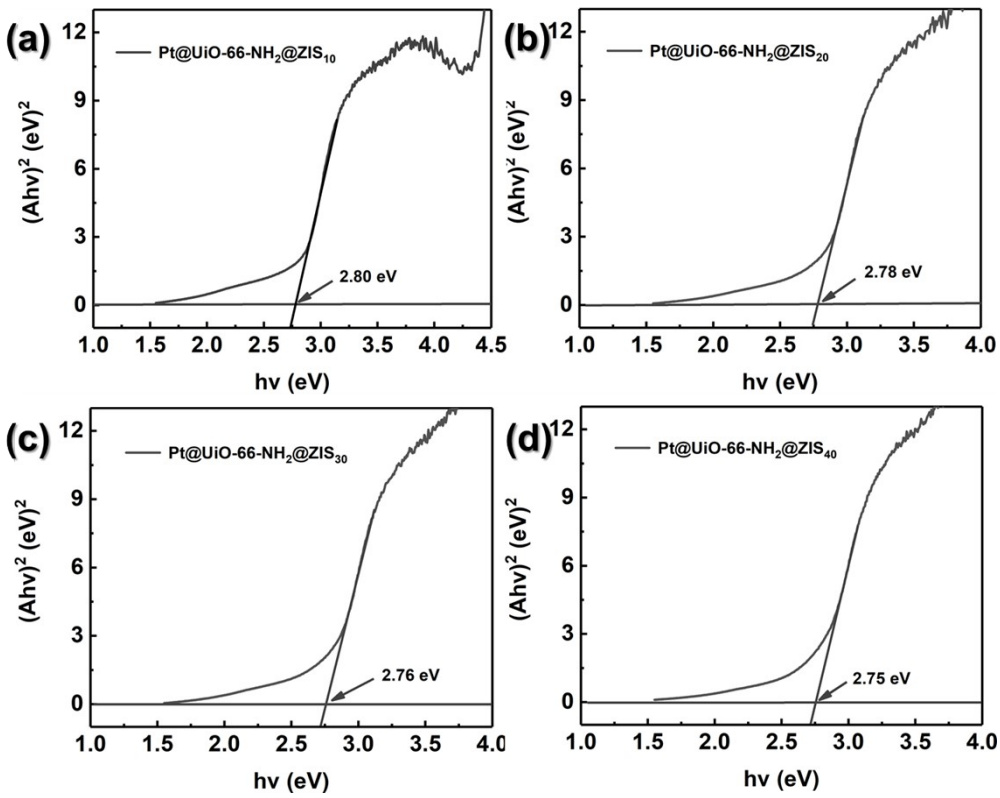

Fig. S7 Calculation of band gap energy of composite materials.

Table S1. Surface area and pore volume parameters of composite materials

Samples	Surface area (m^2 g^{-1})	Pure size (nm)
Pt@UiO-66-NH_2@ZIS_{10}	810.23	0.9344
Pt@UiO-66-NH_2@ZIS_{20}	788.38	0.9248
Pt@UiO-66-NH_2@ZIS_{30}	786.44	0.9041
Pt@UiO-66-NH_2@ZIS_{40}	778.81	0.7848
Pt@UiO-66-NH_2	1048.9	1.0026
UiO-66-NH_2	1490.5	1.212

Table S2. Time-resolved photoluminescence spectra of Pt@UiO-66-NH_2@ZIS_{20} and UiO-66-NH_2.

Samples	**τ**	**A_1**	**A_2**	**τ_1**	**τ_2**
Pt@UiO-66-NH_2@ZIS_{20}	0.84297	0.16994	0.5271	0.843	0.84297
UiO-66-NH_2	0.78239	0.9163	0.99398	0.78238	0.78241

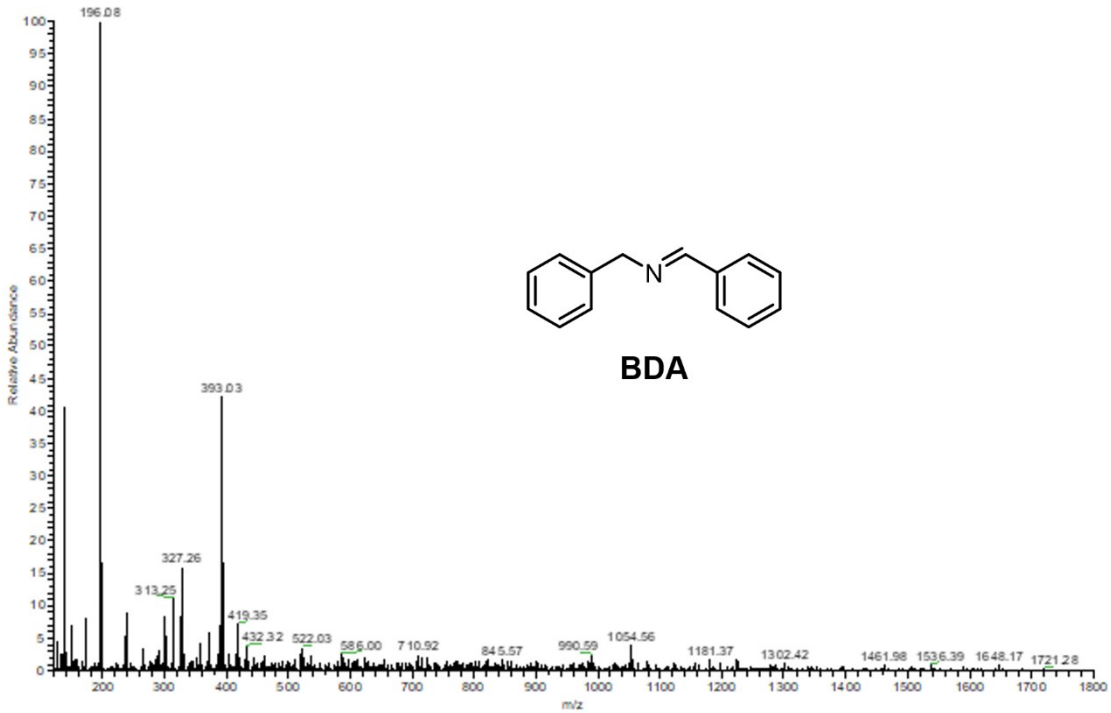

Fig. S8 GC-MS data of reaction product BDA.

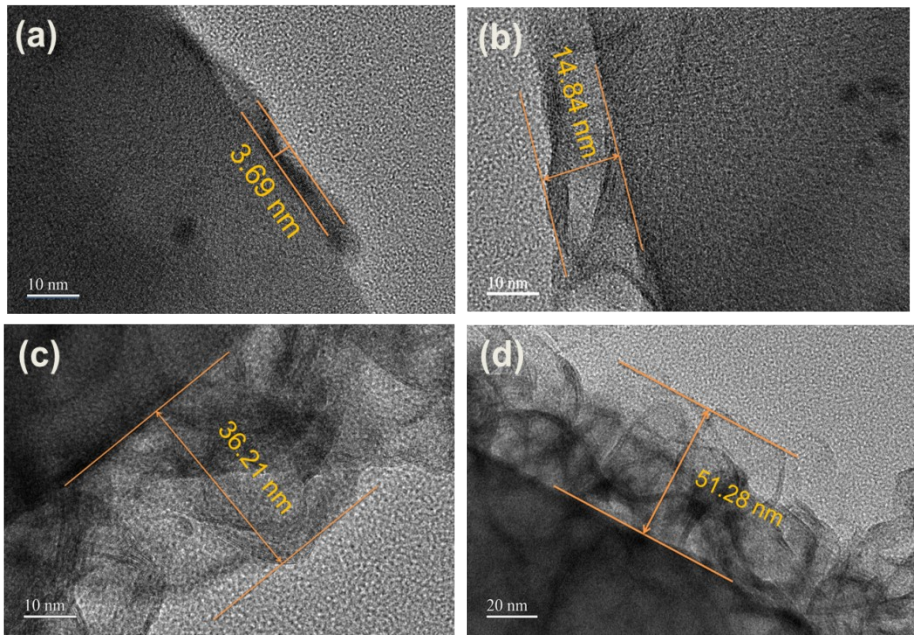

Fig. S9 Thickness of $ZnIn_2S_4$ in the Pt@UiO-66-NH_2@ZIS_X (x=10 (a), 20 (b), 30 (c), 40 (d)).

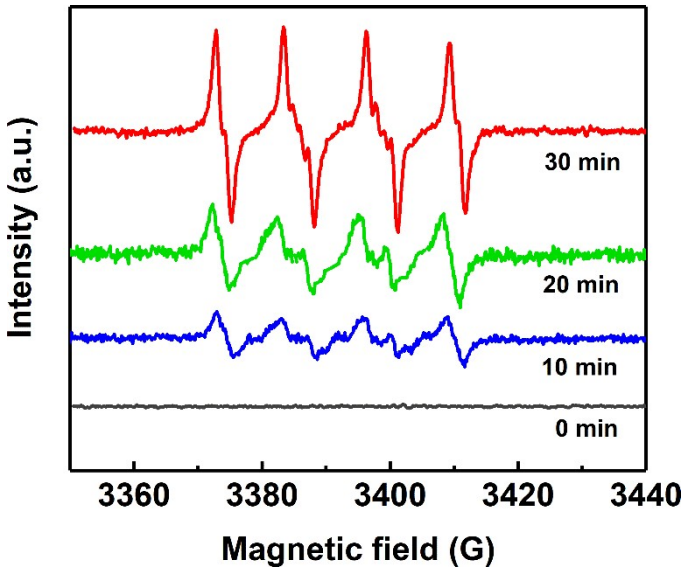

Fig. S10 In situ ESR spectra of Pt@UiO-66-NH_2@ZIS monitored during the photocatalytic reaction with the increase of reaction time. (Testing conditions: catalyst: 20 mg; solvent: acetonitrile (20 mL), water (500 μL), and benzylamine (100 μL), Ar, visible light irradiation, 400 nm < λ < 800 nm, DMPO)

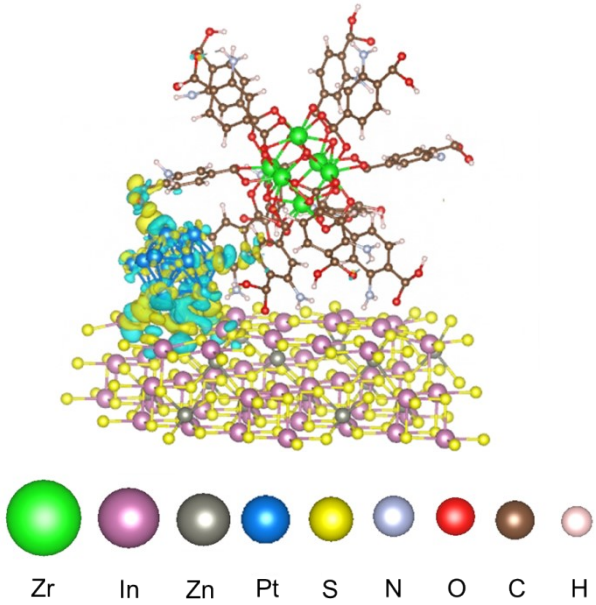

Fig. S11 Charge density difference mappings for Pt@UiO-66-NH_2@$ZnIn_2S_4$ interface

Table S3. Comparisons of photocatalytic performance with different photocatalysts.

Entry	Photocatalyst	Light	H_2 ($\mu mol \cdot g^{-1} \cdot h^{-1}$)	Benzylamine oxidation		Ref.
				Conv.	Sel.	
1	Ni/g-C_3N_4	> 420 nm	596	61.30%	> 99%	6
2	g-C_3N_4/UiO-66-NH_2	> 420 nm	152.2	58.90%	> 99%	7
3	Pt/PCN-777	full spectrum	332	486 $\mu mol \cdot g^{-1} \cdot h^{-1}$	> 99%	8
4	Pt/MOF-808	full spectrum	1.7	128 $\mu mol \cdot g^{-1} \cdot h^{-1}$	> 99%	8
5	Au-Pt-CdS	> 420 nm	778	—	—	9
6	PTCDA-C_3N_4	> 420 nm	—	39%	—	10
7	CdS/$Ti_3C_2T_x$	> 420 nm	219.7	38%	> 99%	11
8	Pt@UiO-66-NH_2@$ZnIn_2S_4$	> 420 nm	850	78%	> 99%	This work

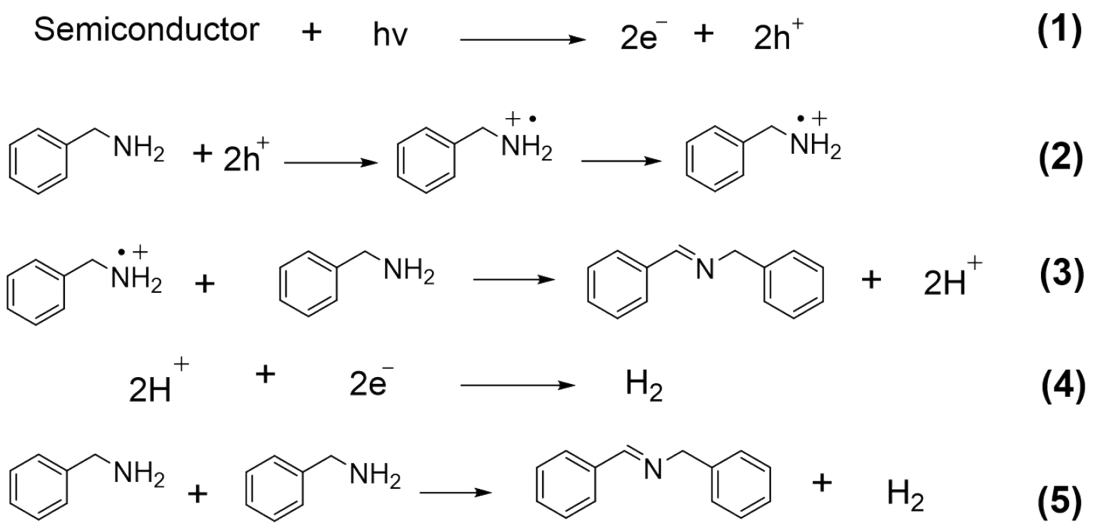

Fig. S12 Proposed reaction pathway for photocatalytic imine production and H_2 evolution over Pd@UiO-66-NH_2@$ZnIn_2S_4$.

References

1. G. Kresse and J. Furthmüller, Efficiency of ab-initio total energy calculations for metals and semiconductors using a plane-wave basis set, *Comput. Mater. Sci.,* 1996, **6**, 15−50.
2. G. Kresse and J. J. Furthmüller, Efficient iterative schemes for ab initio total-energy calculations using a plane-wave basis set, *Phys. Rev. B,* 1996, **54**, 11169−11186.
3. J. P. Perdew, K. Burke and M. Ernzerhof, Generalized gradient approximation made simple, *Phys. Rev. Lett.,* 1996, **77**, 3865−3868.
4. G. Kresse and D. Joubert, From ultrasoft pseudopotentials to the projector augmented-wave method, *Phys. Rev. B,* 1999, **59**, 1758-1775.
5. P. E. Blöchl, Projector augmented-wave method. *Phys. Rev. B*, 1994, **50**, 17953−17979.

6 S. Zhang, X. Qian, J. Yan, K. Chen and J. Huang, Nickel-decorated g-C_3N_4 hollow spheres as an efficient photocatalyst for hydrogen evolution and oxidation of amines to imines, *New J. Chem*., 2020, **44**, 11710-11719.

7 S. Zhang, K. Chen, W. Peng and J. Huang, g-C_3N_4/Uio-66-NH_2 nanocomposites with enhanced visible light photocatalytic activity for hydrogen evolution and oxidation of amines to imines, *New J. Chem*., 2020, **44**, 3052-3061.

8 H. Liu, C. Xu, D. Li and H. Jiang, Photocatalytic hydrogen production coupled with selective benzylamine oxidation over MOF composites, *Angew. Chem., Int. Ed.,* 2018, **57**, 5379-5383.

9 L. Ma, K. Chen, F. Nan, J. Wang, D. Yang, L. Zhou and Q. Wang, Improved hydrogen production of Au-Pt-CdS hetero-Nanostructures by efficient plasmon-induced multipathway electron transfer, *Adv. Funct. Mater.,* 2016, **26**, 6076-6083.

10 Y. Wang, J. Zhou, X. Hao, Y. Wang and Z. Zou, Fabricating direct Z-scheme PTCDA/g-C_3N_4 photocatalyst based on interfacial strong interaction for efficient photooxidation of benzylamine, *Appl. Surf. Sci.,* 2018, **456**, 861-870.

11 H. Wang, P. Hu, J. Zhou, M. B. J. Roeffaers, B. Weng, Y. Wang and H. Ji, Ultrathin 2D/2D $Ti_3C_2T_x$/semiconductor dual-functional photocatalysts for simultaneous imine production and H_2 evolution, *J. Mater. Chem. A*, 2021, **9**, 19984-19993.